Non-Hermitian quantum-like cascaded nonlinear optical frequency conversion and splitting in dissipative media

Mouhamad Al-Mahmoud, Virginie Coda, Andon Rangelov, Germano Montemezzani

Non-Hermitian quantum-like cascaded nonlinear optical frequency conversion and splitting in dissipative media

Mouhamad Al-Mahmoud,[1] Virginie Coda,[2] Andon Rangelov,[1] and Germano Montemezzani[2,*]

[1] Department of Physics, Sofia University, James Bourchier 5 blvd, 1164 Sofia, Bulgaria
[2] Université de Lorraine, CentraleSupélec, LMOPS, F-57000 Metz, France
[*] Corresponding author

E-mail: germano.montemezzani@univ-lorraine.fr

April 2022

Abstract. It is shown that cascaded nonlinear optical frequency conversion over an intermediate wavelength, subjected to dissipation, behaves similarly to population transfer via a decaying state in a three-state non-Hermitian quantum system. The intermediate dissipation leads to a fixed phase relationship between the input signal wave and the wave at the target frequency, what finally stabilizes both waves preventing any spatial oscillation of their powers. The cascaded conversion acts as a stable wave splitter between the input and target waves, the latter being nearly immune to power fluctuations of the pumps . A case of a simultaneous cascade of the sum frequency generation (SFG) and the difference frequency generation (DFG) processes is discussed as an example. A possible implementation, based on aperiodically engineered quasi-phase-matching in Lithium Niobate, is proposed.

Keywords: Nonlinear optics, Cascaded frequency conversion, Non-Hermitian quantum systems, Dissipative media.

1. Introduction

In recent decades, the important analogies existing between quantum mechanics and various domains of classical physics have emphasized the deep connection between these two seemingly contradictory worlds [1]. These analogies are fundamentally connected to the comparable mathematical formalisms governing several phenomena in both fields. Such links are particularly strong with classical optics, which has served as inspiration for several quantum physics formulations. The study and exploitation of analogies between quantum and optical physics is indeed an intense field of research [2, 3] with applications in various areas of photonics, including, among others, waveguide optics [4, 5, 6], polarization optics [7, 8] and nonlinear optics [9, 10, 11, 12]. Some of the latter are inspired by adiabatic techniques developed for quantum population transfer, which includes the celebrated Stimulated Raman Adiabatic Passage (STIRAP) [13, 14, 15] as well as Rapid Adiabatic Passage (RAP) [16, 17] or adiabatic elimination techniques [18, 19]. Others are related to the robust composite pulses approaches, initially developed in the field of nuclear magnetic resonance [20, 21]. While the above examples are related to Hermitian systems that conserve the total energy, much attention has been given recently also to open systems associated to non-Hermitian Hamiltonians and their photonics counterparts involving gain and/or loss. In this context, systems exhibiting the so-called parity-time (PT) symmetry and exceptional points provide new and often counterintuitive ways to control the flow of light [22, 23].

Nonlinear optical frequency conversion of second order [24] in the so called undepleted pump approximation is intrinsically related to population transfer between coupled quantum states. Let us first consider a three-wave mixing interaction involving waves at the frequencies ω_1 and ω_2 (here with $\omega_1 < \omega_2$) and a pump wave at frequency ω_{p1}. It can be easily shown [10, 25] that the basic three-wave mixing processes of sum frequency generation (SFG, $\omega_1 + \omega_{p1} \rightarrow \omega_2$) and difference frequency generation (DFG, $\omega_2 - \omega_{p1} \rightarrow \omega_1$) are analog to the process of inverting a two-state quantum system (for SFG) and to the back-conversion process to the ground state (for DFG), respectively. This kind of analogy holds also in the case of an extension to a two-step cascade of such processes (see Fig. 1, target wave frequency ω_3; second pump ω_{p2}), if they occur simultaneously and if the pumps are still undepleted. However here the analogy is to a three-state quantum system, such as a Λ-type system and not to a two-state system, as depicted schematically in Fig. 2. Indeed, cascaded second-order nonlinear optical processes are quite often employed with the aim of efficiently producing waves at specific frequencies (see for instance [26, 27, 28, 29, 30, 31, 32, 33, 34, 35, 36]). In general, such processes are most useful to generate wavelengths either near or far away from the one of the input signal wave. The first case is often used in connection with wavelength division multiplexing, for instance for power redistribution and all-optical signal processing within the telecom bands. The second is required whenever a direct conversion to the target wavelength in one step is not possible due to lack of phase-matching, or if such a conversion would require the weaker and generally less efficient third order nonlinearity. Phase matching [24] corresponds to the necessity to insure photon momentum conservation across the nonlinear interaction. In the context of cascaded processes, such as those depicted in Fig. 1, one approach consists in separating the two sub-processes, for instance by using two distinct nonlinear optical crystals so that the conversions get spatially separated. In this case, the phase-matching condition can be adjusted independently in each of the crystals for the corresponding sub-process. In the quantum picture of Fig. 2, this solution is equivalent to avoiding any temporal overlap between the coupling of states ψ_1 and ψ_2 through Ω_p, and the coupling of states ψ_2 and ψ_3 through Ω_s. The second approach is the one where all sub-processes occur simultaneously, *i.e.* with temporal overlap in quantum population transfer and with spatial overlap in nonlinear optics. Therefore in this case phase matching should be fulfilled for each of the cascaded processes within a single nonlinear crystal. In the following, we will consider only this simultaneous situation.

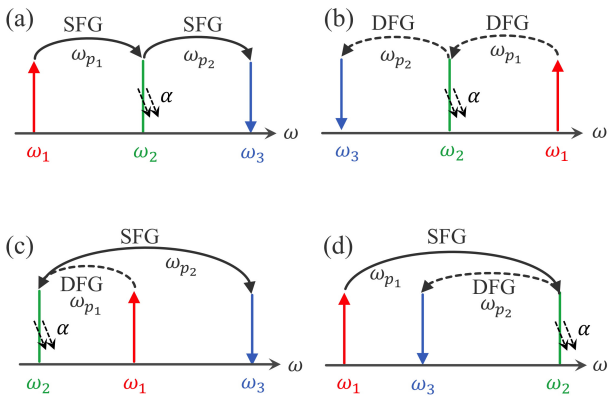

Figure 1. Two-step cascades of three-wave mixing nonlinear optical frequency conversion processes. (a)SFG-SFG, (b) DFG-DFG, (c) DFG-SFG, and (d) SFG-DFG. The frequency ω_1 always corresponds to the input (signal) wave, while ω_3 is the target wave frequency and ω_2 the one of the intermediate wave. ω_{p1} and ω_{p2} are the frequencies of first and second pump waves. The intermediate wave is absorbed by the nonlinear crystal at a rate α (cm^{-1}).

The present work adresses two-step cascaded nonlinear optical interaction in the specific condition

where the wave at the intermediate frequency ω_2 is being strongly dissipated in the medium. It is shown that this situation is fully analogous to the one encountered in a coupled non-Hermitian three-state quantum system, in which the population is decaying out of the system at the intermediate state ψ_2, which was discussed earlier by Vitanov and Stenholm [37]. The dissipation is depicted in Figs. 1 and 2 by the spatial and temporal decay rates α and Γ. It is worth mentioning that the present case is also analog to the recently discussed classical system of three evanescently coupled waveguides that can act as ultra-broadband beam splitter if the intermediate waveguide is strongly dissipative [38]. Here we show that the non-Hermitian nature of the interaction finally leads to a stabilization of the powers in the input (ω_1) and target (ω_3) waves with no power left at the wave at ω_2. The input and target waves acquire a fixed phase relationship and, unlike in the common case in absence of dissipation, they reach a stationary state with no spatial variation of their amplitudes. The system effectively acts as a power splitter between the waves at the frequencies ω_1 and ω_3, with the splitting ratio being adjustable by the strengths of the nonlinear coupling of the two sub-processes. The price to pay is the loss of part of the initial photons at ω_1 due to the dissipation at ω_2. This loss amounts to half of the ω_1-photons if the maximum power at ω_3 is desired. However, significantly lower overall losses are possible for a moderate decrease of this power. Section 2.1 presents the general theoretical aspects for the non-Hermitian three-level quantum system of Fig. 2 under the simplifying assumption that the Rabi frequencies characterizing the two coupling mechanisms are constant in time. The corresponding theory for a five-waves nonlinear interaction of the type SFG-DFG with two pump waves being undepleted is given in Sect. 2.2, the main results are illustrated using normalized coordinates. Finally, a calculated example for a cascaded nonlinear conversion in lithium niobate ($LiNbO_3$) and an intermediate frequency in the near ultraviolet is illustrated in Sect. 3. Here a quasi-phase-matching (QPM) technique able to accommodate the phase mismatch of both the SFG and DFG sub-processes is exploited.

2. Theory

2.1. Decaying three-state quantum system

We first consider a three-state non-Hermitian quantum system as the one depicted on the left side of Fig. 2, where the intermediate level can decay out of the system with a total decay rate $\Gamma \geq 0$. It is assumed that the direct transition between states ψ_1 and ψ_3 is electric-dipole forbidden. This kind of system was

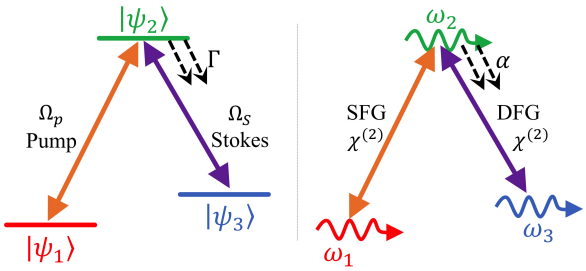

Figure 2. Coupled Λ-type three-state quantum system (left-frame, states ψ_1, ψ_2, and ψ_3) and the analogous classical case of cascaded nonlinear frequency conversion (right-frame, wave frequencies ω_1, ω_2 and ω_3). The quantum states are coupled via the pump and the Stokes Rabi frequencies Ω_p and Ω_s associated to the coupling fields, while the frequency conversion is driven by the second-order susceptibility $\chi^{(2)}$ and the corresponding pump wave amplitudes for the first (assumed here to be SFG) and the second process (DFG). Γ (s^{-1}) and α (cm^{-1}) are the decaying rate of ψ_2 and the amplitude absorption constant of the wave at ω_2, respectively.

discussed in detail in [37]. For the sake of simplicity, here we summarize only the main features that can be put in direct relation with the classical nonlinear optical interaction discussed in the Section 2.2. The overall wave function Ψ that describes the whole system is a linear combination of the three states,

$$\Psi = \sum_{j=1}^{3} c_j(t)\psi_j, \tag{1}$$

where the complex coefficients $c_j(t)$ are the population probability amplitudes of the jth state, with $P_j(t) = c_j(t)^2$ being the probability of occupation of that state. As mentioned above, states ψ_1 and ψ_2 are coupled by a coherent field (for instance a laser field) of Rabi frequency Ω_p (pump field), while states ψ_2 and ψ_3 are coupled by a Stokes field of Rabi frequency Ω_s. As in [37], we consider the case where a detuning Δ is allowed between the oscillation frequencies of the pump and Stokes fields $\omega_{p,s}$ and the corresponding transition frequencies $\omega_{0,p}$ and $\omega_{0,s}$. However, this detuning should be the same for both transitions, i.e. $\Delta = \omega_p - \omega_{0,p} = \omega_s - \omega_{0,s}$, so that the so called two-photon resonance between states ψ_1 and ψ_3 is maintained.

In the rotating-wave approximation, under the above conditions, the probability amplitudes of the three states obey the Schrödinger-type equation [37],

$$i\frac{d}{dt}\begin{bmatrix} c_1 \\ c_2 \\ c_3 \end{bmatrix} = \begin{bmatrix} 0 & \Omega_p & 0 \\ \Omega_p & \Delta - i\Gamma & \Omega_s \\ 0 & \Omega_s & 0 \end{bmatrix}\begin{bmatrix} c_1 \\ c_2 \\ c_3 \end{bmatrix}, \tag{2}$$

where possible spontaneous emission transitions from state ψ_2 to state ψ_1 or ψ_3 has been neglected. A significant role in the dynamics of a three-state system

on two-photon resonance is played by the so-called bright and dark states, that are superpositions of the ground and the target states according to

$$b = \sin\vartheta(t)\psi_1 + \cos\vartheta(t)\psi_3 \ , \tag{3}$$

$$d = \cos\vartheta(t)\psi_1 - \sin\vartheta(t)\psi_3, \tag{4}$$

where the mixing angle $\vartheta(t)$ is defined as

$$\tan\vartheta(t) = \frac{\Omega_p(t)}{\Omega_s(t)} \ . \tag{5}$$

In view of the relation with the nonlinear optical case treated below, one can take the simplifying assumption that the Rabi frequencies Ω_p and Ω_s, and thus also the angle ϑ are constant in time. For the nonlinear interactions, discussed in Sect. 2.2, this will correspond to a nonlinear coupling strength between the waves being constant in space. In alternative to the base used in Eq. (1), the wave function Ψ of the system can be expressed also in a base containing the bright and dark state b and d,

$$\Psi = C_b(t)b + C_2(t)\psi_2 + C_d(t)d \ , \tag{6}$$

where the coefficients in the two bases transform according to the matrix equation

$$\begin{bmatrix} C_b \\ C_2 \\ C_d \end{bmatrix} = \begin{bmatrix} \sin\vartheta & 0 & \cos\vartheta \\ 0 & 1 & 0 \\ \cos\vartheta & 0 & -\sin\vartheta \end{bmatrix} \begin{bmatrix} c_1 \\ c_2 \\ c_3 \end{bmatrix} \ . \tag{7}$$

Here C_b and C_d depict the probability amplitudes for the states b and d, respectively, and $C_2 = c_2$. In the new coordinates and for a constant mixing angle, Eq. (2) turns into the interesting form

$$i\frac{d}{dt}\begin{bmatrix} C_b \\ C_2 \\ C_d \end{bmatrix} = \begin{bmatrix} 0 & \Omega_0 & 0 \\ \Omega_0 & \Delta - i\Gamma & 0 \\ 0 & 0 & 0 \end{bmatrix} \begin{bmatrix} C_b \\ C_2 \\ C_d \end{bmatrix} \ , \tag{8}$$

where $\Omega_0 = \sqrt{\Omega_p^2 + \Omega_s^2}$ is the effective coupling. Inspection of the above equation shows that the states b and ψ_2 are coupled, while the state d is completely decoupled from the other two. Therefore, due to their coupling, the states b and ψ_2 continue to exchange population. However, as a result of the decay of state ψ_2, any population being initially in state b or in state ψ_2 will be lost after a long enough interaction time. In contrast, any population being initially in the dark state d will stay in this state during the whole evolution of the system. As an example, a system initially in state ψ_1 corresponds to the initial conditions $c_1(t=0) = 1$, $C_b(t=0) = \sin\vartheta$ and $C_d(t=0) = \cos\vartheta$. Only this last amplitude does survive the evolution and the back transformation to the base of the three states gives for the final distribution $c_1(t=\infty) = \cos^2\vartheta$, $c_2(t=\infty) = 0$ and $c_3(t=\infty) = -\sin\vartheta\cos\vartheta$. In this case the final population in state ψ_3 is maximized if $\vartheta = \pi/4$ and thus $\Omega_p = \Omega_s$, leading to $|c_1(t=\infty)|^2 = |c_3(t=\infty)|^2 = 1/4$, the remaining $1/2$ of the initial population has been lost by the dissipation is state ψ_2.

2.2. Cascaded Nonlinear Frequency Generation in a Dissipative Medium

The concept of the bright-dark states leading to Eq. (8) can be applied also to the case of a two-step cascaded nonlinear frequency generation system. To well understand the mathematical formalism behind this analogy, we discuss here specifically the case of a SFG process followed by DFG, which corresponds to the case of Fig. 1(d) and to the right panel in Fig. 2. However, this analogy can be applied to all the situations in Fig. 1, provided that the intermediate wave at frequency ω_2 is lossy.

We assume that three waves are initially injected in the nonlinear medium, the input signal wave (at frequency ω_1), and two intense pumps (ω_{p1} and ω_{p2}), with intensities I_{p1} and I_{p2}, respectively. By the SFG process, the signal combines with the first pump to create the intermediate wave at $\omega_2 = \omega_1 + \omega_{p_1}$. Simultaneously, the wave at ω_2 combines with the second pump, by the process $\omega_3 = \omega_2 - \omega_{p_2}$, to generate the target wave by DFG. Hereby, due to dispersion in the nonlinear crystal, the momentum is generally not conserved and the phase-mismatches for SFG (Δk_S) and DFG (Δk_D) are given as

$$\Delta k_S = k_1 + k_{p_1} - k_2 \ , \tag{9a}$$

$$\Delta k_D = k_3 + k_{p_2} - k_2 \ , \tag{9b}$$

where $k_j = \omega_j n_j/c = 2\pi n_j/\lambda_j$ are the wave-numbers of the jth wave ($j = 1, p_1, 2, p_2$ and 3) possessing a vacuum wavelength λ_j and being associated to the refractive index $n_j \equiv n(\omega_j)$. In order to study the spatial evolutions of the number of photons associated to each of the interacting waves, such a system can be described by the symmetrized coupled wave equations for collinear five-wave mixing in the slowly varying envelope approximation [24, 39] as

$$i\frac{d}{dz}A_1 = \widetilde{\Omega}_S A_{p_1}^* A_2 e^{-i\Delta k_S z} \ , \tag{10a}$$

$$i\frac{d}{dz}A_{p_1} = \widetilde{\Omega}_S A_1^* A_2 e^{-i\Delta k_S z} \ , \tag{10b}$$

$$i\frac{d}{dz}A_2 = \widetilde{\Omega}_S A_{p_1} A_1 e^{i\Delta k_S z} + \widetilde{\Omega}_D A_{p_2} A_3 e^{i\Delta k_D z} - i\alpha A_2 \ , \tag{10c}$$

$$i\frac{d}{dz}A_{p_2} = \widetilde{\Omega}_D A_3^* A_2 e^{-i\Delta k_D z} \ , \tag{10d}$$

$$i\frac{d}{dz}A_3 = \widetilde{\Omega}_D A_{p_2}^* A_2 e^{-i\Delta k_D z} \ . \tag{10e}$$

Here the amplitudes A_j are proportional to the light electric fields amplitudes E_j associated to each of

the waves and are defined as $A_j \equiv \sqrt{n_j/\omega_j}E_j$. Importantly, their square module ${A_j}^2$ is proportional to the number of photons Φ_j in the jth wave. The quantities $\widetilde{\Omega}_S$ and $\widetilde{\Omega}_D$ are symmetrized effective nonlinear coupling coefficients for the SFG and DFG processes, respectively,

$$\widetilde{\Omega}_S = 2\frac{d_S}{c}\sqrt{\frac{\omega_1\omega_{p_1}\omega_2}{n_1 n_{p_1} n_2}}\ , \tag{11a}$$

$$\widetilde{\Omega}_D = 2\frac{d_D}{c}\sqrt{\frac{\omega_2\omega_{p_2}\omega_3}{n_2 n_{p_2} n_3}}\ . \tag{11b}$$

The quantities $d_S = \chi^{(2)}(\omega_1, \omega_{p_1}; \omega_2)/2$ and $d_D = \chi^{(2)}(\omega_2, \omega_{p_2}; \omega_3)/2$ are the effective second-order nonlinear coefficients for the type of interaction being considered, with $\chi^{(2)}$ being the corresponding second-order nonlinear susceptibility. In the above coupled equations, a particular attention can be given to Eq. (10c). The last term on the right-hand side describes the dissipation of the intermediate wave at ω_2, while the first two terms show that this wave is alimented on one side by the SFG process $\omega_2 = \omega_1 + \omega_{p_1}$ (first term), but also by the SFG process $\omega_2 = \omega_3 + \omega_{p_2}$ (second term) as the back process of the DFG conversion $\omega_3 = \omega_2 - \omega_{p_2}$. The latter is described by the last equation (10e). Similarly, Eq. (10a) describes the DFG back process $\omega_1 = \omega_2 - \omega_{p_1}$.

In the following we assume that the two pumps are undepleted, with their amplitudes largely exceeding those of the three waves of interest ($|A_{p1,p2}| \gg |A_1|, |A_2|, |A_3|$). This condition cancels the second and the fourth equations in (10), which can be reduced to a system of three coupled equations

$$i\frac{d}{dz}A_1 = \Omega_S A_2 \exp e^{-i\Delta k_S z}\ , \tag{12a}$$

$$i\frac{d}{dz}A_2 = \Omega_S A_1 e^{i\Delta k_S z} + \Omega_D A_3 e^{i\Delta k_D z} - i\alpha A_2\ , \tag{12b}$$

$$i\frac{d}{dz}A_3 = \Omega_D A_2 e^{-i\Delta k_D z}\ , \tag{12c}$$

where the coupling coefficients have been slightly redefined and contain now the amplitudes of the pump waves, $\Omega_S \equiv \widetilde{\Omega}_S A_{p1}$ and $\Omega_D \equiv \widetilde{\Omega}_D A_{p2}$. It is useful to substitute the amplitudes A_j with the phase-shifted amplitudes B_j such that their modules are not modified ($A_j = B_j$), that is

$$A_1(z) = B_1(z)\ , \tag{13a}$$

$$A_2(z) = B_2(z)\exp\left[i\Delta k_S z\right]\ , \tag{13b}$$

$$A_3(z) = B_3(z)\exp\left[-i\left(\Delta k_D - \Delta k_S\right)z\right]\ . \tag{13c}$$

Equations (12) transform then into

$$i\frac{d}{dz}\begin{bmatrix} B_1 \\ B_2 \\ B_3 \end{bmatrix} = \begin{bmatrix} 0 & \Omega_S & 0 \\ \Omega_S & \Delta k_S - i\alpha & \Omega_D \\ 0 & \Omega_D & \Delta k_S - \Delta k_D \end{bmatrix}\begin{bmatrix} B_1 \\ B_2 \\ B_3 \end{bmatrix} \tag{14}$$

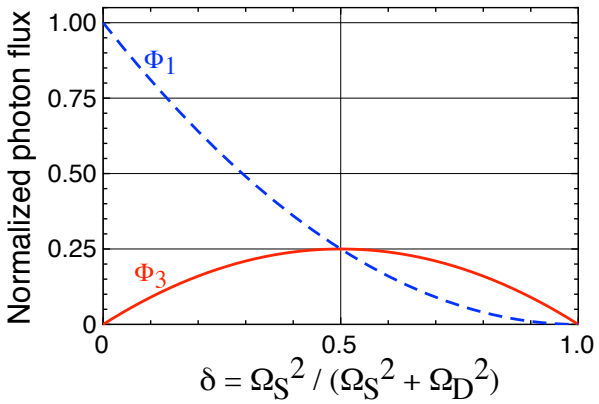

Figure 3. Expected stationary photon fluxes $\Phi_1(z \to \infty)$ (blue dashed line, signal frequency) and $\Phi_3(z \to \infty)$ (red solid line, target frequency) as a function of the overall photon losses δ. The curves are normalized with respect to the initial photon flux at the signal frequency ($\Phi_1(z = 0) = 1$).

By comparing with Eq. (2), it becomes evident that when the last element of the matrix above tends towards zero ($\Delta k_S - \Delta k_D \to 0$), this system becomes fully analog to the problem of the dissipating three-state quantum system discussed in Sect. 2.1. The condition $\Delta k_S - \Delta k_D = 0$ is equivalent to the quantum two-photon resonance condition.

One can therefore follow the same steps as in Sect. 2.1 and transform the vector $\vec{B} = [B_1, B_2, B_3]^T$ containing the wave amplitudes into the bright-dark basis $\vec{C} = [C_b, C_2, C_d]^T$ by undergoing the same transformation as in Eq. (7),

$$\begin{bmatrix} C_b \\ C_2 \\ C_d \end{bmatrix} = \begin{bmatrix} \sin\vartheta & 0 & \cos\vartheta \\ 0 & 1 & 0 \\ \cos\vartheta & 0 & -\sin\vartheta \end{bmatrix}\begin{bmatrix} B_1 \\ B_2 \\ B_3 \end{bmatrix}\ , \tag{15}$$

this time with a mixing angle given as $\tan\vartheta = \Omega_S/\Omega_D$ (instead of Eq. (5)). In full analogy to (8), under this coordinate transformation and for spatially constant couplings Ω_S and Ω_D, Eq. (14) becomes

$$i\frac{d}{dz}\begin{bmatrix} C_b \\ C_2 \\ C_d \end{bmatrix} = \begin{bmatrix} 0 & \Omega_0 & 0 \\ \Omega_0 & \Delta - i\alpha & 0 \\ 0 & 0 & 0 \end{bmatrix}\begin{bmatrix} C_b \\ C_2 \\ C_d \end{bmatrix}\ , \tag{16}$$

with $\Omega_0 \equiv \sqrt{\Omega_S^2 + \Omega_D^2}$ and $\Delta = \Delta k_S = \Delta k_D$. Again, the dark state $C_d = B_1\cos\vartheta - B_3\sin\vartheta$ is completely decoupled from the other two, which are still coupled to each other. For a sufficiently long propagation distance any photon population initially in the bright state C_b or in the state $C_2 = B_2$ will be lost due to the absorption constant α, while the population initially in the dark state is maintained in that state.

If, besides for the pump waves, only the signal wave ω_1 is present at the input we have at the position $z = 0$ following initial conditions, $A_1(0) = B_1(0) = 1$,

$A_2(0) = B_2(0) = C_2(0) = 0$ and $A_3(0) = B_3(0) = 0$, where for practical purposes the input wave amplitude has been normalized to 1. This input field $\vec{B} = [1, 0, 0]^T$ corresponds to a superposition of the bright and dark states with projections given by

$$C_b(0) = \sin\vartheta \ , \tag{17a}$$

$$C_d(0) = \cos\vartheta \ . \tag{17b}$$

The corresponding normalized powers $\Phi_b \equiv {C_b}^2$ and $\Phi_d \equiv {C_d}^2$ in the bright and dark states at $z = 0$ are therefore

$$\Phi_b(0) = \sin^2\vartheta = \frac{\Omega_S^2}{\Omega_S^2 + \Omega_D^2} \equiv \delta \ , \tag{18a}$$

$$\Phi_d(0) = \cos^2\vartheta = \frac{\Omega_D^2}{\Omega_S^2 + \Omega_D^2} = 1 - \delta \ . \tag{18b}$$

We keep in mind that the bright state decays due to the non vanishing coupling to the dissipating intermediate state, so that $C_b(z \to \infty) = \Phi_b(z \to \infty) = 0$. This permits to identify the quantity δ defined in Eq. (18a) as the overall normalized photon loss of the two-step cascaded frequency conversion.

On the other hand, the photons in the dark state are maintained so that $C_d(z \to \infty) = \cos\vartheta$ and $\Phi_d(z \to \infty) = \cos^2\vartheta$. By transforming back to the initial basis of the three waves $(\omega_1, \omega_2, \omega_3)$ by means of the inverse relation to (15) one obtains

$$B_1(z \to \infty) = \cos^2\vartheta \ , \tag{19a}$$

$$B_2(z \to \infty) = 0, \tag{19b}$$

$$B_3(z \to \infty) = -\sin\vartheta\cos\vartheta \ . \tag{19c}$$

The corresponding normalized photon numbers at the signal and target frequencies are therefore

$$\Phi_1(z \to \infty) = \frac{\Omega_D^4}{(\Omega_S^2 + \Omega_D^2)^2} \equiv (1 - \delta)^2 \ , \tag{20a}$$

$$\Phi_3(z \to \infty) = \frac{\Omega_S^2 \Omega_D^2}{(\Omega_S^2 + \Omega_D^2)^2} = \delta(1 - \delta) \ . \tag{20b}$$

Therefore, thanks to the losses of the intermediate wave, the two-step cascaded nonlinear optical process acts as a power splitter between the input wave at ω_1 and the target wave at ω_3. The splitting ratio and the conversion efficiency depend on the ratio of the coupling coefficients Ω_S and Ω_D, and thus on the overall photon losses of the system δ. Figure 3 illustrates the normalized photon numbers at the input and target wavelengths as a function of δ. As can be easily recognized, the maximum number of photons at ω_3 is obtained for $\delta = 0.5$, in which case the two waves contain the same number of photons, each being 25% of the initial number in the input wave.

The above stationary state is reached for a long enough interaction length in the nonlinear crystal. Given a certain crystal length L, it is useful to evaluate the level of absorption α of the intermediate wave and

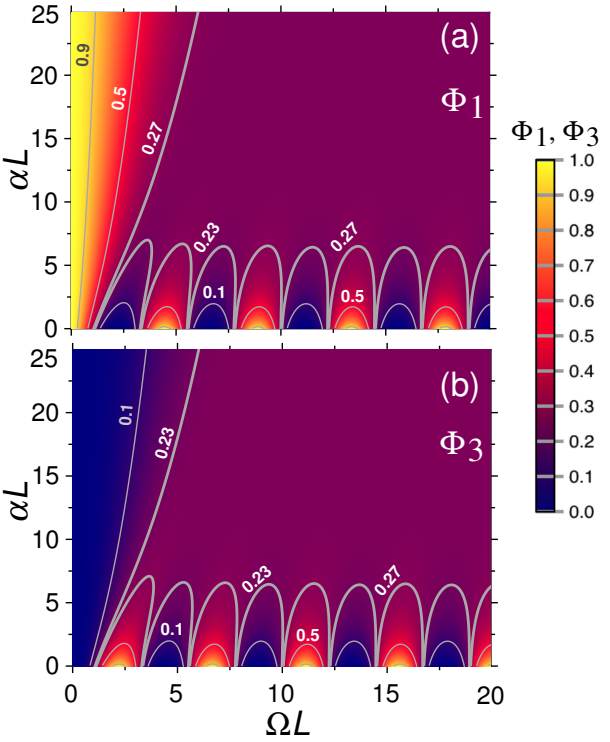

Figure 4. Normalized number of photons $\Phi_1(z = L)$ (a) and $\Phi_3(z = L)$ (b) as a function of the coupling-length product ΩL and of the absorption-length product αL, as obtained by numerical integration of Eq. (14). The coupling coefficients of both processes are supposed equal, $\Omega = \Omega_S = \Omega_D$ and both, SFG and DFG, are supposed to be phase-matched ($\Delta k_S = \Delta k_D = 0$). The color scale gives the number of photons relative to those injected in the input wave (ω_1). The large purple region on the top-right of both frames correspond to the situation of interest in this work, while the power oscillations on the abscissas correspond to the standard case of a vanishing amplitude absorption constant at ω_2, ($\alpha = 0$).

of the coupling of the two nonlinear processes required to reasonably reach this steady-state. To do that we assume, for the sake of simplicity, that phase matching is fulfilled for both SFG and DFG ($\Delta k_S = \Delta k_D = 0$) and that the coupling for the two sub-processes is the same ($\Omega_S = \Omega_D \equiv \Omega$). Figure 4 shows contour plots of the relative number of photons $\Phi_1(L)$ and $\Phi_3(L)$ as a function of the products ΩL and αL, as obtained by direct integration of Eq. (14) under the above assumptions. Within the large purple region on the top right of the two panels the final photon numbers at both frequencies ω_1 and ω_3 are between 23% and 27% of the initially injected ones in the signal wave. It can be recognized that an amplitude absorption constant α of the order of $10/L$ is largely sufficient to be in this regime. At the same time the coupling constant Ω should be at least of the order of $5/L$. Note that, in the whole purple region, the number of photons at the intermediate frequency ω_2 is vanishing small. On the other hand, the conditions on the abscissas of Fig. 4(a)

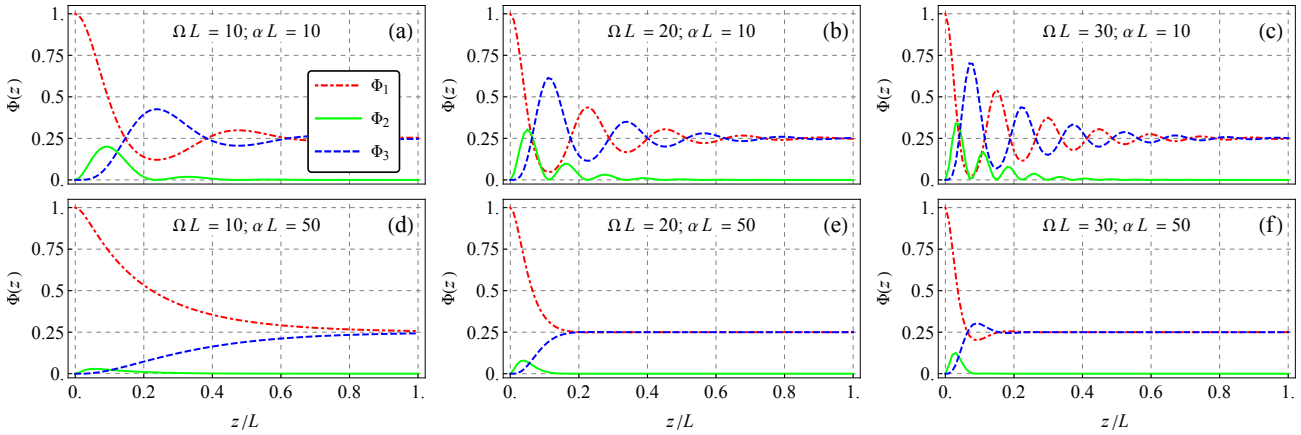

Figure 5. Spatial evolutions of the normalized photon fluxes $\Phi_1(z)$, $\Phi_2(z)$ and $\Phi_3(z)$ for a crystal length L and various values of Ω and α within the purple region of Fig. 4. The same conditions as in Fig. 4 are used. Top raw (a), (b), (c): $\alpha L = 10$; bottom raw (d), (e), (f): $\alpha L = 50$. Left column (a), (d): $\Omega L = 10$; central column (b), (e): $\Omega L = 20$; right column (c), (f): $\Omega L = 30$. All curves reach a final state with $\Phi_1(L) \approx \Phi_3(L) \approx 0.25$.

and Fig. 4(b) correspond to the case $\alpha = 0$, where the intermediate wave would not be dissipated. In this case one gets the expected spatial power oscillation between signal and target wave (Rabi-like oscillations). However, within these spatial transients, a significant power can be also at the intermediate wave (not shown in Fig. 4). In this specific case, a maximum of 50% of the initial photons can be at frequency ω_2, what is associated to ΩL values between the maxima and the minima for the input and target waves, *i.e.* at positions where the contour lines in Fig. 4 reach the abscissa.

It is interesting to look at the spatial evolution towards the final stationary state within the optimum purple regions of Fig. 4. Figure 5 illustrates the quantities $\Phi_j(z)$ along the crystal for various points on the $(\Omega L, \alpha L)$ parameter plane, all belonging to the purple region, thus leading to nearly the same final state. The general feature is that both $\Phi_1(z)$ and $\Phi_3(z)$ show damped spatial oscillations before reaching the steady state at the value 0.25. For a given value of α an increase of Ω increases the number and the frequency of the oscillations. In contrast, for a given value of Ω an increase of α decreases the oscillations and leads generally to a faster stabilization. For sufficiently large α the system becomes overdamped with no oscillations left. This behavior is similar to what observed for several equivalent coupled systems in classical or quantum physics [40].

It is useful to discuss the spatial evolution of the relative phases of the three waves at ω_1, ω_2 and ω_3. We do this with the help of Fig. 6 which corresponds to the case of Fig. 5(b). The reference phase for the signal wave is fixed at $\zeta_1(z) = 0$ by our definition. As can be seen, the generated target wave gets in anti-phase to the signal, so that its phase assumes the value $\zeta_3(z) = \pi$ all along. In contrast, during the damped oscillations the phase ζ_2 of the intermediate wave can assume the values $+\pi/2$ or $-\pi/2$. In the second case the target wave is being amplified at the expense of the signal wave, in the first case it is the other way round. This behavior is the result of the interplay of the SFG and DFG processes for each of the two cascaded conversions. For instance, in the sections where the signal is being re-amplified ($\zeta_2 = +\pi/2$), this occurs by the DFG process $\omega_2 - \omega_{p1} \rightarrow \omega_1$. The relative phase of π between the signal and target waves is valid in the case of perfect phase matching discussed here. It permits to understand better what is happening in the stationary state, where only the so-called dark state survives . Indeed, the intermediate wave is alimented by both SFG processes $\omega_2 = \omega_1 + \omega_{p_1}$ and $\omega_2 = \omega_3 + \omega_{p_2}$ as discussed earlier in connection to Eq. (10c). In the stationary regime, these two processes are equally strong but, being in anti-phase due to the phase $\zeta_3 = \pi$, they lead to a perfect destructive interference at the intermediate wave, which ends up being "dark" . This explains also the apparent paradox that, in the stationary state, there are more photons in the target wave than in the signal wave ($\Phi_3 > \Phi_1$) whenever the second nonlinear process is weaker than the first ($\Omega_D < \Omega_S$), as seen in Fig. 3 for $\delta > 0.5$. This is because the stationary state balance mentioned above can be maintained only if a weaker coupling is counter-balanced by a larger amplitude in the corresponding source wave.

Finally, before addressing a concrete numerical example, we would like to point out that the present approach allows to reach a very stable intensity level of the target wave. Indeed, the loss in the intermediate wave has the effect of stabilizing the output target wave intensities against power fluctuations of the two pumps. Fluctuations of the pump intensities lead to

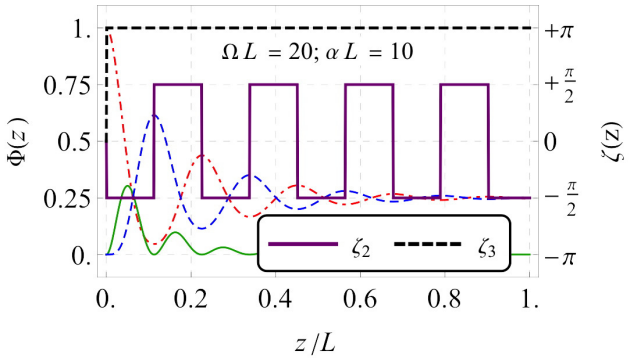

Figure 6. Relative phases of the intermediate wave ($\zeta_2(z)$, purple solid line) and of the target wave ($\zeta_3(z)$, black dashed line) with respect to the phase of the signal wave (right-hand scale). The evolution is for the same case as in Fig. 5(b). The normalized photon fluxes $\Phi(z)$ (left-hand scale) are reproduced as well. The red dash-dotted curve, the green solid curve and the blue dashed curve give $\Phi_1(z)$, $\Phi_2(z)$ and $\Phi_3(z)$, respectively.

variations of the coupling coefficients Ω_S and/or Ω_D and thus of the normalized photon loss δ in (18a). However, as can be easily recognized in Fig. 3, a change of δ has only a little effect on the photon flux Φ_3 in (20b) in the case where this flux is balanced to the one of the signal wave ($\delta \approx 0.5$). Under these conditions, a fluctuation of one of the two pump intensities by 5% with respect to the other would lead to a fluctuation in the intensity of the wave at frequency ω_3 by only $\approx$ 0.06% of the maximum value. If the relative fluctuation would be 10% the target wave fluctuation is still less than 0.3%. In comparison, the corresponding fluctuations in this last case in absence of dissipation can exceed 50%.

3. Example for engineered lithium niobate

The above calculations were presented in a general normalized way and were based on the assumption that both processes, SFG and DFG in our case, are phase-matched in the crystal of interest. In practice such a phase matching is not easy to achieve. Even though birefringent phase matching [24, 39] may be possible for each of the two processes, it is very unlikely to be able to achieve it for both processes in a single configuration (propagation direction inside the crystal and/or temperature). The same is true for the standard quasi-phase-matching (QPM) method [24] which entails splitting the crystal into small periodic segments with alternating inversion of the sign of the nonlinear coefficients d_S and d_D in (11), and thus also of the signs of Ω_S and Ω_D in (12). Usually the QPM method can address only a single nonlinear process, but a modification aimed at a simultaneous phase matching of both processes in cascade will be discussed below.

Our calculated example to illustrate possible implementations of the concept is based on the $LiNbO_3$ nonlinear crystal. This material is one of the most used one in nonlinear optics. It combines reasonably large nonlinearity with the ease of growth and with the possibility of reversing the sign of the local nonlinearity by electric-field induced ferroelectric domain reversal [41]. We assume that the second-order nonlinear tensor element driving both processes is the same and, by neglecting its possible weak dispersion, we can take $d_0 = d_S = d_D = d_{333} = 27$ pm/V [41]. The nonlinear optical wave interaction is calculated over a crystal length $L = 20$ mm and the phase mismatch is calculated based on the values of the refractive indices at the temperature $T = 300$ K. Because the predominant absorption of such a crystal occurs in the ultraviolet spectral range, the set of frequencies is chosen such that the intermediate wave is in this range. The chosen wavelengths of the five interacting waves are

$$\lambda_1^{532\text{nm}} + \lambda_{p_1}^{800\text{nm}} \rightarrow \lambda_2^{319.5\text{nm}} , \quad (21a)$$

$$\lambda_2^{319.5\text{nm}} - \lambda_{p_2}^{1064\text{nm}} \rightarrow \lambda_3^{456.6\text{nm}} , \quad (21b)$$

where the first line gives the SFG and the second line the DFG process. All the interacting waves are supposed to be extraordinarily polarized (in direction of the crystal z-axis), which justifies the use of the largest nonlinear optical tensor element d_{333}.

As mentioned above, standard QPM generally addresses a single nonlinear optical frequency conversion process at once. The idea is to compensate the primary phase-mismatch Δk_S (or Δk_D) with an additional wavevector K_S (or K_D) in order to fulfill the following relationships

$$\overline{\Delta k}_S = \Delta k_S + K_S = \Delta k_S + m_S \frac{2\pi}{\Lambda_S} = 0 , \quad (22a)$$

$$\overline{\Delta k}_D = \Delta k_D + K_D = \Delta k_D + m_D \frac{2\pi}{\Lambda_D} = 0 , \quad (22b)$$

where m_S and m_D are the integer QPM orders, and Λ_S and Λ_D are the QPM modulation periods for the SFG and the DFG processes, respectively. Based on the refractive index data in [42], for our set of interacting wavelengths in $LiNbO_3$, one finds for the first-order QPM periods, $\Lambda_S = 1.06$ μm and $\Lambda_D = 1.18$ μm at 300 K. In this material, the QPM structures are realized by inversion of ferroelectric domains and for such short periods the domain configuration lack a sufficient long-time stability, it is therefore useful to use longer periods by going to higher orders m_S and m_D. The use of QPM implies a reduction of the effective nonlinearity of the sample by a factor $G_m = (2/\pi m) \sin(m\pi/2)$ that depends on its order m. This form clearly shows that only odd orders are of interest. The quantity G_m actually correspond to the Fourier coefficient of the term with modulation wavevector $|\Delta k_S|$ (or $|\Delta k_D|$) in

the Fourier series of the QPM square modulation with period Λ_S (or Λ_D).

In order to be able to phase match simultaneously both the SFG and the DFG processes one has to structure the crystal in such a way that both Fourier components $|\Delta k_S|$ and $|\Delta k_D|$ are present at the same time and with similar amplitudes of their coefficients. This kind of problem is not uncommon and is encountered whenever the simultaneous phase-matching of two distinct nonlinear processes is desired. We may define the average phase mismatch at order m as

$$\overline{k}_m = \frac{1}{m}\frac{\Delta k_S + \Delta k_D}{2} \tag{23}$$

and the half-difference of the individual phase mismatches as

$$\Delta k = \frac{\Delta k_S - \Delta k_D}{2}. \tag{24}$$

The simultaneous phase matching of both processes can then be reached by using the aperiodic modulation function $\delta(z)$ of the sign of the nonlinear coefficient defined as [43]

$$\delta(z) = \frac{d(z)}{d_0} = \text{sign}\left[\sin\left(\overline{k}_m z\right)\sin\left(\Delta k z\right)\right], \tag{25}$$

which is associated to a common reduction factor

$$\overline{G}_m = \frac{1}{m}\left(\frac{2}{\pi}\right)^2 \tag{26}$$

of the effective nonlinearity of SFG and DFG, which are taken at the same order m. The quantity $\overline{G}_m$ is a factor $2/\pi$ smaller than G_m, the case where only one of the processes is addressed individually. It is important, in this context, to leave the difference Δk at order 1 as given in (24), this can be done because this quantity is generally small.

As mentioned above, the maximum photon flux for the target wave is found under the condition $\vartheta = \pi/4$ and thus $\Omega_S = \Omega_D$. This allows to establish a specific relationship for the ratio of the intensities of the pumps I_{p2} and I_{p1} required to satisfy this condition,

$$\rho \equiv \frac{I_{p2}}{I_{p1}} = \frac{n_{p2}n_3}{n_{p1}n_1}\frac{\lambda_3}{\lambda_1} \approx \frac{\lambda_3}{\lambda_1}, \tag{27}$$

where the last approximation can be made in case of weak refractive index dispersion in the spectral range of the pumps and of the signal and target waves. In our specific example $\rho \approx 0.86$ provided that a perfect implementation of the aperiodic QPM structure given in Eq. (25) can be achieved in practice.

The correct working of the aperiodic QPM structuring for the simultaneous phase matching can be verified by numerically integrating the initial coupled equations (12) while keeping the mismatch terms Δk_S and Δk_D in the exponentials and switching the sign of the nonlinear coefficients $\tilde{\Omega}_S$ and $\tilde{\Omega}_D$ at each domain boundary, what is shown in Fig. 7. The first panel,

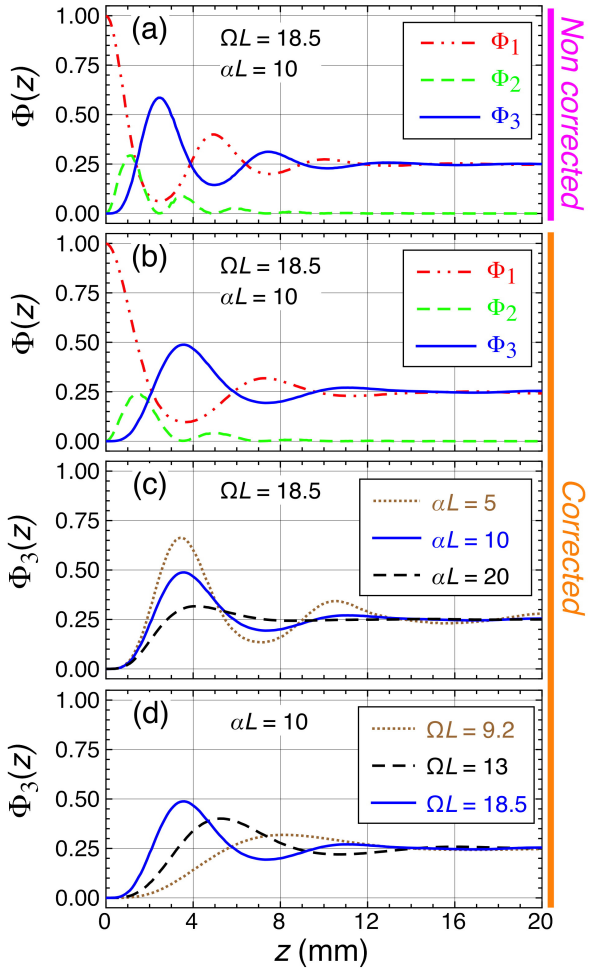

Figure 7. Calculated spatial evolution of the normalized photon fluxes for the case of a two-step conversion in a $LiNbO_3$ crystal subjected to an aperiodic domain structuring. In (a) the domains are designed according to Eq. (25) while in (b)-(d) they are corrected for a minimum domain size of 5 μm (see text for details). The curves are obtained by a direct numerical integration of Eq. (12) by conserving all phase mismatch terms and switching the sign of the nonlinear coupling coefficients at each domain boundary. Panels (a) and (b) give the normalized photon fluxes for the signal wave (Φ_1, red dashed-dotted curve), the intermediate wave (Φ_2, green dashed curve) and the target wave (Φ_3, blue solid curve) over a distance $L = 20$ mm and for $\alpha = 0.5$ mm^{-1} and thus $\alpha L = 10$. The uncorrected coupling-length product $\Omega L = 18.5$ corresponds to pump intensities $I_{p1} = 1$ GW/cm^2 and $I_{p2} = 0.69$ GW/cm^2 in (a) or $I_{p2} = 0.69$ GW/cm^2 in (b), see text. Panel (c) shows $\Phi_3(z)$ for the same coupling strength as in (b) but for three values of the absorption given in the inset. Panel (d) gives again $\Phi_3(z)$ for $\alpha L = 10$ with three values of the coupling. For the brown dotted curve, both pump wave intensities are reduced by a factor 4 with respect to cases (b) and (c), while for the black dashed curve they are reduced by half. The solid blue curve is identical in the three corrected panels (b) to (d).

Fig. 7(a), shows the photon flux evolution for the waves ω_1, ω_2 and ω_3 for our example within a 20 mm long aperiodic structured $LiNbO_3$ crystal. The structuring is supposed to be by domain reversal following Eq. (25) at the order $m = 9$. The value of $\Omega L = 18.5$ ($\Omega = 0.925$ mm^{-1}) corresponds to the nonlinear coupling coefficient Ω_S for SFG within each individual domain multiplied by the nominal reduction factor $\overline{G}_m$ in (26) for pump intensity $I_{p1} = 1$ GW/cm^2, *i.e.* $\Omega = \Omega_S \overline{G}_m$. Figure 7(a) is for $I_{p2} = \rho I_{p1} = 0.86$ GW/cm^2 and shows that the aperiodic structuring works well and give results fully consistent with the ideal normalized case discussed in Sect. 2.2 (see for instance Fig. 5(b)).

However, the aperiodic structuring according to (25) contains also some domains which are very short and, as a consequence, are generally unstable in $LiNbO_3$ under normal experimental conditions. To face this problem one can set a lower limit for the domain size and perform a correction of the structure. This consist in flipping any domain smaller than a minimum value so that these domains are merged with the two adjacent ones. In our calculations, we have chosen a (conservative) minimum value of 5 μm, which is well consistent with available commercial $LiNbO_3$ QPM products. Note that the correction procedure of the aperiodic design is performed sequentially from the entrance to the output of the structure. Panels (b), (c) and (d) in Fig. 7 present this corrected case. It is worth noting that the corrections favors slightly the DFG process over SFG. This is because the chance of making a correction on DFG is somewhat lower due to the smaller phase mismatch in our example. This has the consequence that the balance of the effective nonlinearities (25% of photons at the signal and target wave) is obtained for a ratio $I_{p2}/I_{p1} \approx 0.69$ being used for Fig. 7(b-d). This is smaller than the value of ρ calculated with (27) and used for Fig. 7(a). It can be recognized that the results obtained with the corrected structure (Fig. 7(b)) and the uncorrected one (Fig. 7(a)) are very similar. The lower oscillation spatial frequency in Fig. 7(b) is associated to a decrease of the effective nonlinearity below the value $\Omega L = 18.5$, as a result of the correction process, the latter being calculated in absence of any corrections. We have also verified that, in presence of the aperiodic structuring, at the spatial steady state, the target and signal waves still possess a fixed phase relationship. The phase difference, though, differs from the value of π found for perfect phase matching (see Fig. 6). This is the result of the additional effective phase shifts associated on one hand to the QPM process and, on the other hand, to the domain correction. Nevertheless, the destructive interference, discussed in Sect. 2.2, of the steady-state contributions of signal and target waves to the wave at frequency ω_2 is still at work.

The curves in Fig. 7(a-b) are for an amplitude absorption constant $\alpha = 0.5$ mm^{-1}, which is actually a bit smaller than the one expected for our configuration. The wavelength $\lambda_2 = 319.5$ nm of the intermediate wave corresponds closely to the ultraviolet band edge cut-off λ_c for congruently grown $LiNbO_3$. Indeed, according to Refs. [41, 44] this cut-off, defined at an intensity absorption constant level $2\alpha = 20$ cm^{-1} ($\alpha = 1$ mm^{-1}), is at $\lambda_c = 320$ nm. The corresponding situation ($\alpha L = 20$) for the evolution of the target wave flux $\Phi_3(z)$ is shown as black dashed line in Fig. 7(c). The latter also shows the case ($\alpha L = 5$) which would occur if the wavelength λ_2 would have been chosen a few nanometers longer. Figure 7(c) reproduces well the behavior expected under variation of the absorption constant already predicted in Fig. 5. The same expected equivalence can be seen also for the case of Fig. 7(d) that shows the effect of diminishing the coupling strength by a decrease of the intensities of both pump waves with respect to the case of Fig. 7(b). We can therefore conclude, that our example, involving the full integration of the initial coupled equations in an aperiodically engineered crystal, entirely confirms the predictions put forward in Sect. 2.2.

4. Conclusion

We have shown that cascaded nonlinear optical frequency conversion with dissipation at the intermediate frequency and quantum population transfer via a decaying state in a three-state coupled system behave similarly. The nonlinear optical system essentially acts as a stable, adjustable and partially lossy wave splitter between the input signal wave and the wave at the target wavelength. The splitting ratio is tunable by the coupling strengths associated to the two cascaded sub-processes. Among the possible configurations, we have treated specifically the one of a cascaded SFG-DFG conversion process. As an example, it was shown that a QPM-type aperiodic structure with corrections for too short domains can serve for a realistic implementation in $LiNbO_3$, with the intermediate dissipating wave being in the ultraviolet. However, the concept can be applied to several other materials, such as for instance aperiodically poled $KTiOPO_4$ (KTP) [45, 46], and to other processes, such as DFG-SFG, SFG-SFG, or DFG-DFG, provided that the intermediate wave is sufficiently absorbed. The required dissipation level to reach the spatially stable output regime in terms of the amplitude absorption constant α was shown to be of the order $5 - 10$ over the length of the nonlinear medium.

The present approach may be useful to split an input wave into two waves of different wavelengths, with stable relative intensities, or to reach a very stable

intensity level of the target wave, with highly reduced fluctuations, as compared to the fluctuations of the pump waves. It is also worth mentioning that the approach presented here works independently on the initial intensity of the input wave. The concept can therefore be applied also in the case of single photon or few photons input in the context of quantum optics.

Acknowledgements

This work was supported by EU Horizon-2020 ITN project LIMQUET (contract number 765075) and by Sofia University Grant 80-10-55/10.05.2022. We dedicate this work to the inspiring memory of Bruce Shore.

References

[1] Dragoman D and Dragoman M 2013 *Quantum-classical analogies* (Springer Science & Business Media)
[2] Longhi S 2009 *Laser & Photon. Rev.* **3** 243–261
[3] Feng L, El-Ganainy R and Ge L 2017 *Nat. Photonics* **11** 752–762
[4] Longhi S, Della Valle G, Ornigotti M and Laporta P 2007 *Phys. Rev. B* **76** 201101
[5] Menchon-Enrich R, Llobera A, Vila-Planas J, Cadarso V J, Mompart J and Ahufinger V 2013 *Light: Sci. & Appl.* **2** e90
[6] Oukraou H, Vittadello L, Coda V, Ciret C, Alonzo M, Rangelov A A, Vitanov N V and Montemezzani G 2017 *Phys. Rev. A* **95** 023811
[7] Ardavan A 2007 *New J. Phys.* **9** 24
[8] Dimova E, Rangelov A and Kyoseva E 2015 *Photon. Res.* **3** 177–179
[9] Porat G and Arie A 2012 *JOSA B* **29** 2901–2909
[10] Suchowski H, Porat G and Arie A 2014 *Laser & Photon. Rev.* **8** 333–367
[11] Erlich Y, Rangelov A, Montemezzani G and Suchowski H 2019 *Opt. Lett.* **44** 3837–3840
[12] Li F, Zhang Z, Wan T, Zhang H and Chen C 2022 *Opt. Commun.* **502** 127427
[13] Gaubatz U, Rudecki P, Schiemann S and Bergmann K 1990 *J. Chem. Phys.* **92** 5363–5376
[14] Vitanov N V, Rangelov A A, Shore B W and Bergmann K 2017 *Rev. Mod. Phys.* **89** 015006
[15] Shore B W 2017 *Advances in Optics and Photonics* **9** 563–719
[16] Liedenbaum C, Stolte S and Reuss J 1989 *Phys. Rep.* **178** 1–24
[17] Vitanov N V, Halfmann T, Shore B W and Bergmann K 2001 *Ann. Rev. Phys. Chem.* **52** 763–809
[18] Lugiato L A, Mandel P and Narducci L M 1984 *Phys. Rev. A* **29** 1438–1452
[19] Brion E, Pedersen L H and Mølmer K 2007 *J. Phys. A* **40** 1033–1043
[20] Levitt M H 1986 *Prog. Nucl. Magn. Reson. Spectrosc.* **18** 61–122
[21] Shaka A J and Pines A 1987 *J. Magn. Reson.* **71** 495–503
[22] El-Ganainy R, Makris K G, Khajavikhan M, Musslimani Z H, Rotter S and Christodoulides D N 2018 *Nat. Phys.* **14** 11–19
[23] Özdemir Ş K, Rotter S, Nori F and Yang L 2019 *Nat. Mater.* **18** 783–798
[24] Boyd R W 2008 *Nonlinear optics* 3rd ed (Burlington: Academic Press)
[25] Rangelov A A, Vitanov N V and Montemezzani G 2014 *Opt. Lett.* **39** 2959–2962
[26] Saltiel S M, Sukhorukov A A and Kivshar Y S 2005 Chapter 1 - Multistep parametric processes in nonlinear optics (*Progress in Optics* vol 47) ed Wolf E (Elsevier) pp 1–73
[27] Chou M, Brener I, Fejer M, Chaban E and Christman S 1999 *IEEE Photon. Technol. Lett.* **11** 653–655
[28] Chen B and Xu C Q 2004 *IEEE J. Quantum Electron.* **40** 256–261
[29] Lee Y L, Yu B A, Jung C, Noh Y C, Lee J and Ko D K 2005 *Opt. Express* **13** 2988–2993
[30] Gao S, Yang C, Xiao X, Tian Y, You Z and Jin G 2007 *J. Light. Technol.* **25** 710–718
[31] Wang J, Sun J and Sun Q 2007 *Opt. Express* **15** 1690–1699
[32] Bogoni A, Wu X, Fazal I and Willner A E 2009 *Opt. Lett.* **34** 1825–1827
[33] Conforti M, Baronio F, Angelis C D, Marangoni M and Cerullo G 2011 *J. Opt. Soc. Am. B* **28** 892–895
[34] Smirnova D A and Solntsev A S 2015 *Phys. Rev. B* **92** 155410
[35] Chen H, Huang H, Wu F, Wang F and Shen D 2020 *Opt. Express* **28** 30726–30735
[36] Lu C, Li H, Qiu J, Zhang Y, Liu S, Zheng Y and Chen X 2022 *Opt. Express* **30** 1381–1387
[37] Vitanov N and Stenholm S 1997 *Phys. Rev. A* **56** 1463
[38] Alrifai R, Coda V, Peltier J, Rangelov A A and Montemezzani G 2021 *Phys. Rev. A* **103** 023527
[39] Shen Y R 2003 *The Principles of Nonlinear Optics* (Hoboken: Wiley)
[40] Shore B W and Vitanov N V 2006 *Contemp. Phys.* **47** 341–362
[41] Nikogosyan D N 2006 *Nonlinear optical crystals: a complete survey* (New York: Springer Science & Business Media)
[42] Edwards G J and Lawrence M 1984 *Opt. Quant. Electron.* **16** 373–375
[43] Carrillo-Fuentes M, Cudney R S, Lee S H and Kwon O P 2020 *Opt. Express* **28** 24444–24451
[44] Kovacs L, Ruschhaupt G, Polgar K, Corradi G and Wöhlecke M 1997 *Appl. Phys. Lett.* **70** 2801–2803
[45] Karlsson H and Laurell F 1997 *Appl. Phys. Lett.* **71** 3474–3476
[46] Lagatsky A A, Brown C T A, Sibbett W, Holmgren S J, Canalias C, Pasiskevicius V, Laurell F and Rafailov E U 2007 *Opt. Express* **15** 1155–1160